The throughput of the modified nonpersistent ICMA/CD is

$$S = \alpha G e^{-\alpha G}/[\alpha + \alpha G e^{-\alpha G} + \gamma(1 - e^{-\alpha G} - \alpha G e^{-\alpha G})] \quad (2)$$

and that of the previous nonpersistent ICMA/CD was derived[2] as

$$S = aGe^{-(a+b)G}/[a + aGe^{-(a+b)G} + c(1 - e^{-aG} - aGe^{-(a+b)G})] \quad (3)$$

The channel capacity C is the maximally achievable throughput obtained at an optimum value of the offered traffic G. Let C_i, C_m and C_p denote the channel capacities of our improved, the modified and the previous protocols, respectively. An example of the calculated channel capacities with some fixed parameters is shown in Fig. 2.

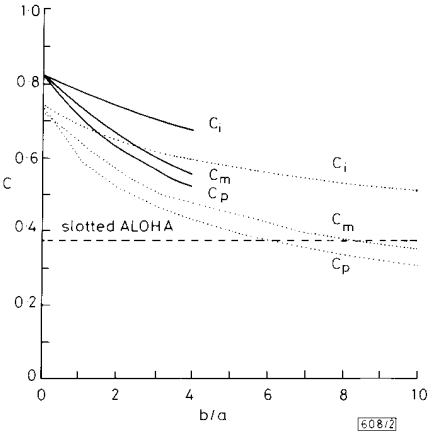

Fig. 2 *Channel capacity against b/a for various slotted nonpersistent protocols*

——— $c = 0{\cdot}2$ (with collision detection)
····· $c = 1{\cdot}0$ (without collision detection)
$a = 0{\cdot}05$

Analytic results and conclusion: The throughput of a slotted CSMA is well known to be better than that of unslotted case. C_p is always worse than C_m because the previous ICMA protocol[1] is similar to the unslotted CSMA as the ratio of b/a becomes smaller. Both C_p and C_m of the ICMA scheme will be inferior by 0·368 to the slotted ALOHA, when b/a becomes larger than 6 for C_p and 8 for C_m, as shown in Fig. 2.

Our protocol has the best channel capacity among them. The performance improvement of ICMA and ICMA/CD results from fully utilising the information of the slotted broadcast channel to reduce collisions. We note that the improved performance of our protocol is relatively insensitive to the packet detection delay than the previous protocol.[1]

E. CHOI

Department of Electrical Engineering
Korea Advanced Institute of Science and Technology
PO Box 150, Chongyangni, Seoul 131, Korea

M. KIM

School of Electrical Engineering
Cornell University
Phillips Hall, Ithaca, New York 14853, USA

& Department of Electrical Engineering
Korea Advanced Institute of Science and Technology
PO Box 150, Chongyangni, Seoul 131, Korea

13th March 1989

References

1 MURASE, A., and IMAMURA, K.: 'Idle-signal casting multiple access with collision detection (ICMA/CD) for land mobile radio', *IEEE Trans.*, 1987, **VT-36**, pp. 45–50

2 ADACHI, F., OHNO, K., and KITAGAWA, M.: 'Performance analysis of ICMA/CD multiple-access for a packet mobile radio', *Electron. Lett.*, 1988, **24**, pp. 469–471

OPTICAL PHASELOCK RECEIVER WITH MULTIGIGAHERTZ SIGNAL BANDWIDTH

Indexing terms: Optical communications, Optical receivers, Semiconductor lasers

We have built a balanced *pin*FET receiver which employs two signal amplification paths for homodyne detection of multigigabit-per-second, pilot-carrier PSK optical signals. Using narrow-line 1·51 μm semiconductor lasers, we have employed this receiver to phaselock a local oscillator to a 295 pW pilot carrier with 8° RMS phase error.

Introduction: Homodyne detection of PSK optical signals offers, in theory, the best sensitivity of any binary signalling technique, as well as high channel packing density, reduced receiver thermal noise and minimum required receiver bandwidth. In the wavelength range of interest for high-speed, fibre-optic communication systems, HeNe lasers have been used to demonstrate a 140 Mb/s[1] pilot-carrier homodyne system, and an external-cavity semiconductor laser (ECL) has been used to construct a homodyne optical phaselock loop (OPLL).[2] The advantages of homodyne make it increasingly attractive at higher bit rates. Unlike previous demonstrations, this work addresses the requirements of a receiver for multigigabit-per-second pilot-carrier systems. Such a receiver must pass the coherently demodulated data, and must also provide a low-noise, DC-coupled, phase-error signal for the carrier-recovery OPLL. We start with a proven, high-speed, front-end design which is well suited for the demodulated data signal, but which is not usable as a phase detector because: (*a*) it uses HEMTs which have excessive low-frequency noise; (*b*) it has a lower-than-optimum transimpedance gain; (*c*) it uses AC interstage coupling. To provide a phase-error signal, we add additional circuitry which extracts its signal at nodes which, from the point of view of the high-speed front end, are at AC ground.

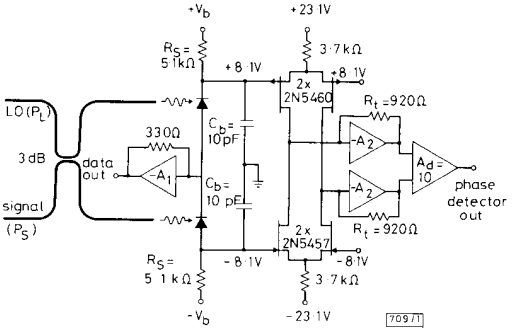

Fig. 1 *Schematic diagram of phaselock balanced receiver*

Circuit design: The receiver (Fig. 1) contains two 75 μm-diameter, planar GaInAs *pin* photodiodes which are illuminated by the two outputs of a fibre 3 dB coupler. The data branch consists of a HEMT-based, 330 Ω transimpedance circuit[3] which has total input capacitance of 0·8 pF (0·2 pF from the input HEMT and 0·3 pF from each *pin*). It is sufficient to bypass each *pin* with $C_b = 10$ pF to ground.

The phase detector extracts its signal from the sensor resistors R_s placed in series with the bias of each *pin*. The signal from each sensor resistor is amplified by a differential JFET pair (all four JFETs have matched transconductance g_m). The following stages consist of DC-20 MHz transimpedance amplifiers and a DC-20 MHz differential amplifier. The low-frequency response of the phase detector is given by

$$K_d\left(\frac{V}{rad}\right) = \frac{2\eta e\lambda}{hc}\sqrt{P_S P_L}\, R_s g_m R_t A_d \quad (1)$$

For the parameters $\eta = 0{\cdot}78$, $\lambda = 1{\cdot}51$ μm, $P_S = 295$ pW, $P_L = 695$ μW and $g_m = 2{\cdot}43$ mmho, eqn. 1 gives $K_d =$

98 mV/rad. This circuit has its first pole at a frequency $f_p = 1/[2\pi R_s(C_b + C_i)]$, where $C_i = 4$ pF is the JFET input capacitance.

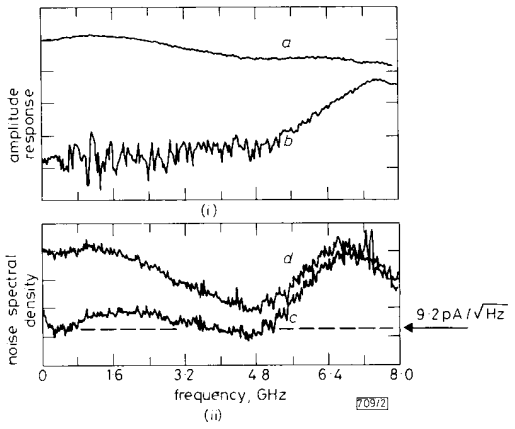

Fig. 2 (i) *Data branch amplitude response*
a Differential
b Common-mode
(ii) *Noise density*
c Thermal
d Thermal plus shot

Receiver measurements: Figs. 2*a* and *b* show the amplitude response of the receiver data branch, recorded using an intensity-modulated optical signal introduced into one input port of the 3 dB coupler, and normalised to the response of a *pin* detector having a 3 dB bandwidth of 15 GHz. With only one *pin* illuminated, the differential response (Fig. 2*a*) exhibits a 3 dB bandwidth of 3·4 GHz and smoothly varying, substantial response to 8 GHz. This receiver is thus usable for bit rates of up to 5 Gb/s, and higher bit rates with equalisation. With both *pins* equally illuminated, the common-mode response (Fig. 2*b*) exhibits excellent rejection to frequencies above 5 GHz. The thermal-noise density of the data branch is shown in Fig. 2*c*, and Fig. 2*d* shows the shot noise added by a photocurrent of 675 μA. The low-frequency thermal-noise density is 9·2 pA/$\sqrt{(}$Hz), compared with the 7·1 pA/$\sqrt{(}$Hz) Johnson noise of the 330 Ω feedback resistor. With this relatively small local-oscillator power, estimated thermal-noise penalties are 1·7, 2·2 and 3·5 dB at bit rates of 2, 4 and 8 Gb/s, respectively.

Fig. 3 presents analogous measurements for the phase-detector output. The differential response (Fig. 3*a*) exhibits the expected 3 dB bandwidth of 2·2 MHz, and the common-mode response (Fig. 3*b*) is suitably small. The thermal-noise density is shown in Fig. 3*c*, and Fig. 3*d* shows the shot noise added by a 600 μA photocurrent. The observed thermal noise of 2·7 pA/$\sqrt{(}$Hz) is close to the 2·5 pA/$\sqrt{(}$Hz) expected from the two 5100 Ω resistors. When the receiver is illuminated with a total local-oscillator power $P_L = 695\,\mu$W and no signal, the phase detector exhibits a total output drift of 10 mV/5 min which, for the parameters given above, represents a 6° phase drift. This is caused by mechanical creep of the fibre-*pin* coupling, and could be improved by pigtailing of the receiver or through automatic balancing.[2] We employed angled fibre ends and tilted *pin* detectors so that the receiver optical return loss exceeded 50 dB, ensuring that Rayleigh-scattered, reflected local-oscillator light will not dominate the loop phase error.[2]

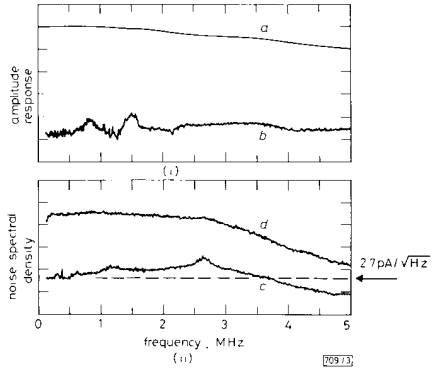

Fig. 3 (i) *Phase detector amplitude response*
a Differential
b Common-mode
(ii) *Noise density*
c Thermal
d Thermal plus shot

Phaselock experiment: Operation of the phase detector has been tested in a second-order OPLL. The optical sources were 1·51 μm ECLs with 4 kHz beat linewidth. The phase error signal was processed by a lead-lag integrator[4] and fed back to the injection current of the local oscillator, which had a two-contact chip to allow fast frequency modulation. We employed a pilot carrier power of $P_S = 295$ pW, and loop parameters[4] were set at $\omega_n = 590$ krad/s, $\zeta = 0{\cdot}72$, and $K_v = 1{\cdot}3 \times 10^9\,s^{-1}$. Locking was observed for periods of up to 30 minutes, limited by drift of the phase detector balance.

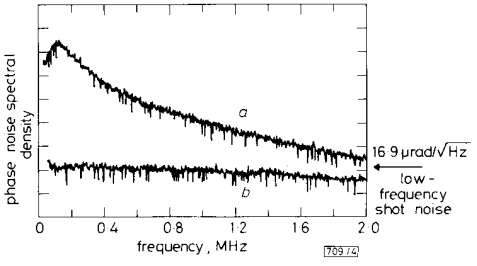

Fig. 4
a Spectral density of phase error signal in locked loop
b Shot noise with no signal present

Fig. 4*a* presents the spectral density of the phase error signal in the locked loop. This is to be contrasted with the open-loop phase-error density, i.e. the Lorentzian beat spectrum, which rises to a large value at DC. Below a frequency breakpoint of order $\omega_n/2\pi$ ($\sim$100 kHz), Fig. 4*a* exhibits a phase-error density which decreases rapidly with decreasing frequency, as expected. Above that breakpoint, the phase-error density is essentially the same as that in the open loop. Integration of the phase error density yields an RMS phase error of 8°, close to the 7° expected.[5] Addition of a PSK signal with power as much as 6 dB above the quantum limit is expected to increase the RMS phase error to $\leq 11°$, owing to data-to-phaselock crosstalk.[5] This phase error should be sufficiently small to allow error-free detection.

Acknowledgments: The assistance of P. J. Fitzgerald, J. S. Perrino, G. E. Bodeep and C. A. Burrus is appreciated. Discussions with B. Glance, P. S. Henry and R. A. Linke are gratefully acknowledged.

J. M. KAHN *21st March 1989*
AT&T Bell Laboratories
Crawford Hill Laboratory, Holmdel, NJ 07733, USA

B. L. KASPER
AT&T Bell Laboratories
Solid State Technology Center, Breinigsville, PA 18031-9359, USA

K. J. POLLOCK
180 East End Avenue
New York, NY 10128, USA

References

1 MALYON, D. J.: 'Digital fibre transmission using optical homodyne detection', *Electron. Lett.*, **20**, 1984, pp. 281–283

2 MALYON, D. J., SMITH, D. W., and WYATT, R.: 'Semiconductor laser homodyne optical phase-locked loop', *Electron. Lett.*, 1986, **22**, pp. 421–422
3 KASPER, B. L., TALMAN, J. R., and GNAUCK, A. H.: To be published.
4 GARDNER, F. M.: 'Phaselock techniques' (John Wiley and Sons, 1979)
5 KAZOVSKY, L. G.: 'Balanced phase-locked loops for optical homodyne receivers: performance analysis, design considerations, and laser linewidth requirements', *J. Lightwave Technol.*, 1986, **LT-4**, pp. 182–195

EXTREMELY LOW LOSS InP/GaInAsP RIB WAVEGUIDES

Indexing terms: Waveguides, Polarisation, Semiconductor growth

We have fabricated InP/GaInAsP rib waveguides with losses as low as 0·18 dB/cm for the TE polarisation and 0·26 dB/cm for the TM polarisation. The length of the waveguides was 28 mm. These losses are measured with the Fabry–Perot method and repeated for different lengths of the waveguide for determining the reflection coefficient.

Introduction: Waveguides on InP substrates are very interesting because of their potential use in switches, modulators, etc. and for integration with lasers, detectors and electronics. However, complex circuits can only be realised if low loss waveguides can be fabricated over large areas in this material. We have investigated a waveguide structure (Fig. 1) consisting of a quaternary GaInAsP layer sandwiched between two cladding InP layers. The lateral confinement is realised by etching a rib structure with a reactive ion etching (RIE) process. This structure is very suitable for the fabrication of low loss waveguides as it needs only one epitaxial step and the rib does not reach the quaternary layer, avoiding a strong influence of possible roughness caused by the etching.

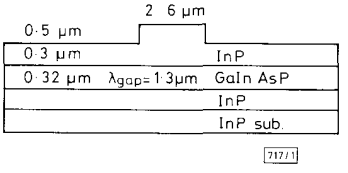

Fig. 1 *Schematic view of double heterostructure rib waveguides*

The loss of these waveguides, measured with the Fabry–Perot (FP) method, turned out to be $0{\cdot}18 \pm 0{\cdot}02$ dB/cm. To our knowledge this is the lowest value ever reported for waveguides on InP substrates. Earlier publications mentioned a loss of 0·4 dB/cm for either buried waveguides[1] and rib waveguides.[2]

Fabrication: The layers are grown by low-pressure organometallic vapour-phase epitaxy on a 2 inch semi-insulating InP substrate. All layers are not intentionally doped and have a residual carrier concentration of 2×10^{15} cm^{-3}. The GaInAsP layer has a gap wavelength of 1·30 μm and a thickness of 0·32 μm. The top InP layer with a thickness of 0·8 μm is etched 0·5 μm deep with an RIE process using $Cl_2/CH_4/H_2/Ar$ gases. The ridges were varied in width between 2 and 5·5 μm and were protected with a SiO_2 layer during the etching. This results in rib waveguides with a difference in refractive index of 9×10^{-3} in the lateral direction and ensures single-mode behaviour for waveguides smaller than 4 μm. The waveguides are positioned exactly along the [0$\bar{1}$1] crystal direction to obtain perpendicular endfacets.

The Fabry–Perot method: An often-used method for measuring the losses of semiconductor waveguides is the cut-back method. However, this method is destructive and not accurate when the losses of the waveguides are much smaller than the injection losses. The Fabry–Perot method does not have these disadvantages and is well suited for characterising low loss waveguides. The losses are deducted from the maximum and minimum intensities that appear owing to the interference between the injected light and the light reflected on both endfacets.[3] The attenuation of the waveguide is given by

$$-\alpha L = \ln\left(\frac{1-\sqrt{1-\gamma^2}}{\gamma R}\right)$$

with L the length of the waveguide, R the reflection coefficient of the endfacet and

$$\gamma = \frac{I_{max} - I_{min}}{I_{max} + I_{min}}$$

I_{max} and I_{min} are the maximum and minimum intensities of the FP fringes.

The only uncertainty is the reflection coefficient which must be known very accurately if the waveguides have low losses. It is already known[4] that the reflection coefficient cannot be simply derived from the effective refractive index in the Fresnel formula. Owing to the large numerical aperture of the waveguide, we will find a larger value for the TE mode and a smaller value for TM mode. Buus[4] derived an approximative analytical formula for the reflectivity of the facets of rib structure lasers. If we use this formula for our rib waveguides ($N_{eff} = 3{\cdot}2537$), we obtain $R_{TE} = 0{\cdot}342$, while the effective refractive index will lead to $R_0 = 0{\cdot}281$.

We have experimentally determined the reflection coefficient and the losses by applying the FP method for waveguides of different lengths. After measuring γ for waveguides with length 28 mm, the substrate is cleaved into two parts 8 and 20 mm long, which are measured too. For one set of waveguides, we found a reflection coefficient for the TE polarisation of $R_{TE} = 0{\cdot}359 \pm 0{\cdot}002$ and for another set we obtained $R_{TE} = 0{\cdot}366 \pm 0{\cdot}002$. These values are the average values deducted from 3 waveguides within a set. As expected for waveguides with small lateral confinement, we found the same reflection coefficient for waveguides with different width. The difference between the sets can be explained by a variation of 0·01 μm in the layer thickness. The experimentally determined reflection coefficient R_{TE} is larger than the one calculated with the Buus formula. Similar results have been already reported for InP rib waveguides.[2] For the set first mentioned, we found in the same manner a reflection coefficient R_{TM} for the TM mode of 0·250.

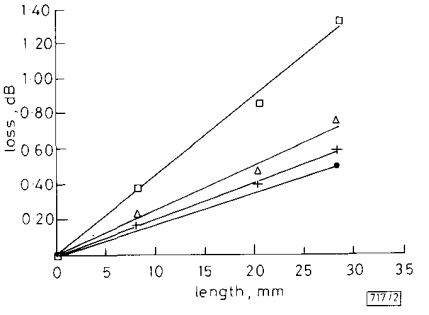

Fig. 2 *Losses of several waveguides of set 1 as a function of length*
Reflection coefficient of 0·359 (TE mode) is used for all waveguides
● 0·18 dB/cm
□ 0·47 dB/cm
△ 0·26 dB/cm
\+ 0·20 dB/cm

Results: Either TE or TM light from a HeNe laser emitting at 1·52 μm is injected into the waveguides. The Fabry–Perot fringes are induced by placing a small heating coil above the substrate. The results of some waveguides of set 1 ($R_{TE} = 0{\cdot}349$) can be seen in Fig. 2. Sometimes inconsistent results are obtained after cleaving the substrate. This is most probably owing to the nonperfect endfacets or the non-homogeneous distributed loss. The smallest loss for a 28 mm waveguide was $0{\cdot}18 \pm 0{\cdot}02$ dB/cm. The losses of the TM mode for the same